

Spatially Resolved Conductivity of Rectangular Interconnects considering Surface Scattering - Part I: Physical Modeling

Xinkang Chen, and Sumeet Kumar Gupta, Senior *Member*, IEEE

Abstract— Accurate modeling of interconnect conductivity is important for performance evaluation of chips in advanced technologies. Surface scattering in interconnects is usually treated by using Fuchs-Sondheimer (FS) approach. While the FS model offer explicit inclusion of the physical parameters, it lacks spatial dependence of conductivity across the interconnect cross-section. To capture the space-dependency of conductivity, an empirical modeling approach based on “cosh” function has been proposed, but it lacks physical insights. In this work, we present a 2D spatially resolved FS (SRFS) model for rectangular interconnects derived from the Boltzmann transport equations. The proposed SRFS model for surface scattering offers both spatial dependence and explicit relation of conductivity to physical parameters such as mean free path and specularity of electrons (p) and interconnect geometry. The solution obtained from our SRFS model is exact for diffusive scattering. For specular scattering, we approximate the solution and show that the average conductivity obtained from SRFS shows a good match with the previous models for a general value of p . We highlight the importance of physics-based spatially resolved conductivity model by showing the differences in the spatial profiles between the proposed physical approach and the previous empirical approach.

Index Terms—Boltzmann transport equation, Fuchs-Sondheimer, interconnect, 2D resistivity model

This work was supported, in part, by the NEW materials for Logic, Memory and InTerconnectS (NEWLIMITS) Center funded by the Semiconductor Research Corporation (SRC)/National Institute of Standards and Technology (NIST) under Award 70NANB17H041. (Corresponding author: Xinkang Chen.)

Xinkang Chen and Sumeet Kumar Gupta are with the School of Electrical and Computer Engineering, Purdue University, West Lafayette, IN 47907 USA (e-mail: chen3030@purdue.edu; guptask@purdue.edu).

Color versions of one or more of the figures in this article are available online at <http://ieeexplore.ieee.org>

I. INTRODUCTION

Technology scaling has been amongst the most important drivers for the advancement of electronic devices, leading to continual improvements in their speed, energy efficiency and integration density. However, technology scaling comes with its own set of challenges and therefore, mandates innovations to counter them. At the device level, scalable transistor topologies such as FinFETs and nano-sheet transistors^{1,2} are being explored that can manage short channel effects at miniaturized dimensions and provide high transistor performance and energy efficiency. With the transistor designs continually improving, a major bottleneck for technology scaling has emerged in the interconnect design³.

The challenges in the interconnect scaling are manifold. Reducing the interconnect pitch and width increases their resistance due to lower cross-sectional area (A_w) across which the current conduction takes place. But, more importantly, the resistivity (ρ_w) also increases with width scaling due to increase in the sidewall scattering⁴. Both these factors increase the resistance per unit length for the line metals ($r_{METAL} = \rho_w / A_w$) as well as the resistance of the vias (R_{VIA}). This issue is further aggravated in standard interconnect topologies which utilize thin barrier and/or liner layers to mitigate the electromigration in copper (Cu)^{5,6}. The barrier/liner layers do not scale proportionally with technology scaling, leading to the active conduction area that is lower than the footprint of the interconnects. This, in turn, further increases the sidewall scattering. To counter this, alternate interconnect materials (that can be utilized with thinner or no barrier/liner layers)⁷⁻⁹, novel liner/barrier materials (that offer effective barrier functionalities at ultra-thin dimensions)¹⁰ and more scalable interconnect topologies are being explored¹¹.

To understand the relative pros and cons of various interconnect materials and topologies (that drive their adoption in a technology), modeling their conductivity is highly important. To that end, several modeling approaches have been proposed before. The sidewall scattering is usually treated using the well-known Fuchs-Sondheimer (FS) theory¹². This approach has been used to model the resistivity of thin film¹², square wires with diffusive scattering¹³ and circular wires¹⁴. Another important scattering mechanism due to grain boundaries is captured using the Mayadas-Shatzkes (MS) theory¹⁵. With these theories forming the bedrock of

> REPLACE THIS LINE WITH YOUR MANUSCRIPT ID NUMBER (DOUBLE-CLICK HERE TO EDIT) <

conductivity modeling, several other works have utilized variants of FS and MS models to estimate the conductivity in scaled technologies^{16–18}.

Another important approach for sidewall scattering was proposed in¹⁹, in which the wire resistivity have been obtained based on kinetic-theory arguments. For wires with square/rectangular cross-section, this approach yields an exact result for perfectly diffusive surface scattering (specularity $p=0$). However, for general p ($p \neq 0$), the exact solution is challenging to obtain for rectangular wires²⁰. Thus, for general p , the work¹⁹ proposed an infinite series expansion shown in to obtain resistivity for a rectangular wire.

However, one limitation of the sidewall scattering models in most of the existing works is that the conductivity is not spatially resolved but is an average value across the whole cross section²¹. While this limitation is not that significant for the characterization of thin films or modeling wires with ideal geometries (which was the main target of the previous works^{13,21}), modern interconnect structures need models that can predict the spatially dependent conductivity. One reason for this is that the lithography, etching and deposition of the interconnects lead to a taper structure²², with wider width at the top and narrower width at the bottom. As a result, the vertical current path in the vias is non-trivial, especially in the presence of the barrier/liner layers, as shown in Fig. 1. The current spreading¹⁸ necessitates the understanding of how conductivity is distributed across the cross-section.

A notable exception to various interconnect modeling works that does consider the spatial dependence of conductivity accounting for sidewall scattering²³. In this work, the authors use an empirical approach using a “cosh” function to model the conductivity as a function of the x - and y - location in the cross-sectional area of the interconnect. However, being an empirical approach, this technique lacks the physical insights that the FS theory provides.

In this paper, we bridge the gap between the FS approach and the “cosh”-based model²³ by obtaining a spatially resolved model for interconnect conductivity while retaining the physical insights. We derive the spatial dependence of the conductivity of rectangular/square wires (such as vias – Fig. 1) based on the FS theory. For $p=0$ the solution obtained from our conductivity model is exact and consistent with the FS theory. For $p \neq 0$, we propose some approximations and present a spatially resolved conductivity model for a general p . The main contributions of this work are summarized as follows:

- We derive an expression for spatially resolved FS (SRFS) conductivity for rectangular interconnects based on Boltzmann transport equation (BTE) for diffusive surface scattering ($p=0$). The model comprises of physical parameters such as electron mean free path (λ_0) and interconnect width/height.
- Based on this, we propose an approximate solution for spatially resolved conductivity for specular scattering (generic p) and validate our approach by comparing the average conductivity across the cross-section with previous works^{19,24}.

- We compare the proposed model with the previous “cosh”-based modeling approach²³, highlighting the importance of the physics-based spatial resolution of conductivity.

II. BACKGROUND

A. Fuchs-Sondheimer (FS) theory

The Fuchs-Sondheimer (FS)¹² theory is the most popular approach to model the effect of surface scattering on the conductivity of metals based on the Boltzmann transport equation (BTE). In this section, we provide a brief overview of the FS approach.

Let us start with BTE for quasi-free electrons, which, in the presence of an electric field (E) can be written as (1):

$$-\frac{q\vec{E}}{m_{eff}} \cdot \nabla_v f + \vec{v} \cdot \nabla_r f = -\frac{f - f_0}{\tau} \quad (1)$$

Here, f and f_0 are the general and equilibrium distribution functions of the electrons, respectively, q is the electronic charge, m_{eff} is the effective mass of the electrons, v is the electronic velocity, τ is the relaxation time, ∇_v is the gradient operator with respect to v and ∇_r represents the spatial gradient operator.

The solution of (1) can be used to obtain the current density J as

$$\vec{J} = -2q \left(\frac{m_{eff}}{h}\right)^3 \int \vec{v} f d\vec{v} = -2q \left(\frac{m_{eff}}{h}\right)^3 \int \vec{v} \Delta f d\vec{v} \quad (2)$$

where h is the Planck’s constant and $\Delta f = f - f_0$ is the deviation of the electron distribution function from its equilibrium value.

1) Thin Films

For the thin film conductivity considering surface scattering, the approach²¹ utilized (1) and (2) to analyze a metal film of thickness a along with z -direction with E -field in, say, x direction (E_x) – Fig. 2. For a purely diffusive surface scattering, Δf (from (1)) is obtained as

$$\Delta f^+ = \frac{q\tau E_x}{m_{eff}} \frac{\partial f_0}{\partial v_x} \left(1 - e^{-\frac{z}{\tau v_z}}\right) \quad \text{for } v_z > 0 \quad (3)$$

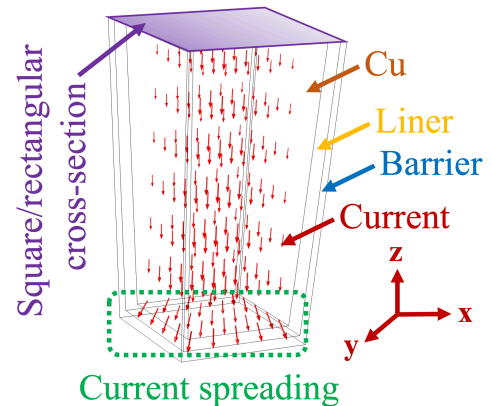


Fig. 1. Tapered via structure with copper conductor and barrier/liner, showing non-trivial current transport (such as current spreading effect at the bottom of the via).

> REPLACE THIS LINE WITH YOUR MANUSCRIPT ID NUMBER (DOUBLE-CLICK HERE TO EDIT) <

$$\Delta f^- = \frac{q\tau E_x}{m_{eff}} \frac{\partial f_0}{\partial v_x} \left(1 - e^{-\frac{a-z}{\tau v_z}}\right) \quad \text{for } v_z < 0$$

Here, v_z and v_x represent the components of the electron velocity along the film thickness (z) and along the electric field (x); and Δf^+ and Δf^- are for electrons with $v_z > 0$ and $v_z < 0$, respectively. Using (2) and (3), the current density (J_x) can be calculated as

$$J_x(z) = -\frac{2q^2 m_{eff}^2 E_z}{h^3} \int_0^\infty dv \int_0^{2\pi} \tau v^3 \cos^2(\Phi) \frac{\partial f_0}{\partial v} d\Phi \times \left[\int_0^{\pi/2} \sin^3(\theta) \left(1 - e^{-\frac{z}{\tau v \cos(\theta)}}\right) d\theta + \int_{\pi/2}^\pi \sin^3(\theta) \left(1 - e^{-\frac{a-z}{\tau v \cos(\theta)}}\right) d\theta \right] \quad (4)$$

Here, the spherical coordinates have been used: $v = |\vec{v}|$; $v_z = v \cos(\theta)$; $v_x = v \sin(\theta) \cos(\Phi)$;

Next, a degenerate electron gas is assumed, which implies that for any function $g(v)$, the following holds.

$$\int_0^\infty g(v) \frac{\partial f_0}{\partial v} dv = -g(\tilde{v}) \quad (5)$$

Here, \tilde{v} is the electron velocity at the Fermi surface.

Note, the scattering rate (τ) and \tilde{v} are related to the mean free path of the electrons (λ_0) by

$$\lambda_0 = \tau \tilde{v} \quad (6)$$

Using (5) and (6) in (4), dividing J_x by E_x and averaging along the z -direction, average conductivity accounting for surface scattering can be obtained.

$$\sigma = \frac{1}{a E_x} \int_0^a J_x(z) dz = \sigma_0 \left[1 - \frac{3\lambda_0}{2a} \int_0^{\pi/2} \sin^3(\theta) \cos(\theta) \left(1 - e^{-\frac{a}{\lambda_0 \cos(\theta)}}\right) d\theta \right] \quad (7)$$

Here, σ_0 is the bulk conductivity given by

$$\sigma_0 = \frac{8\pi q^2 m_{eff}^2 \tilde{v}^2}{3 h^3} \lambda_0 \quad (8)$$

A general expression for the conductivity considering both inelastic (diffusive) and elastic (specular) scattering at the surfaces has also been derived²¹. For this, specularity (p) is defined as the fraction of electrons that are scattered elastically. For this general case, (3) is modified to

$$\Delta f^+ = \frac{q\tau E_x}{m_{eff}} \frac{\partial f_0}{\partial v_x} \left(1 - \frac{1-p}{1-p e^{-a/\tau v_z}} e^{-\frac{z}{\tau v_z}}\right) \quad \text{for } v_z > 0$$

$$\Delta f^- = \frac{q\tau E_x}{m_{eff}} \frac{\partial f_0}{\partial v_x} \left(1 - \frac{1-p}{1-p e^{a/\tau v_z}} e^{-\frac{a-z}{\tau v_z}}\right) \quad \text{for } v_z < 0 \quad (9)$$

Following the same procedure as before, the conductivity is obtained as

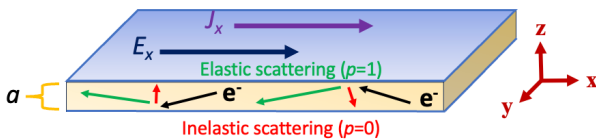


Fig. 2. Thin film structure used for modeling showing fully elastic (specularity $p=1$) or inelastic scattering ($p=0$) when electron hits the top and bottom surfaces.

$$\sigma = \sigma_0 \left[1 - \frac{3\lambda_0}{2a} (1-p) \int_0^{\pi/2} \frac{\sin^3(\theta) \cos(\theta) \left(1 - e^{-\frac{a}{\lambda_0 \cos(\theta)}}\right)}{1 - p e^{-\frac{a}{\lambda_0 \cos(\theta)}}} d\theta \right] \quad (10)$$

The authors²¹ also derive simplified expressions for (7) and (10) for various limiting conditions (such as $a \ll \lambda_0$ and $a \gg \lambda_0$), which have been utilized by many subsequent works^{16,17,25}.

2) Wire with square cross-section

Following the FS theory, the authors¹³ have derived the conductivity considering surface scattering in square wires. In this case, let us assume that the electric field and the current flow is along the z -direction and the wire has width= a and height= $b=a$ (along the x - and y - directions, respectively) – Fig. 3 (next page). Accounting for scattering for the four surfaces of the wire, the following expressions are obtained for Δf considering purely diffusive scattering ($p=0$).

$$\Delta f^{++} = \frac{q\tau E_z}{m_{eff}} \frac{\partial f_0}{\partial v_z} \left(1 - e^{-\frac{\min(\frac{x}{v_x}, \frac{y}{v_y})}{\tau}}\right) \quad \text{for } v_x > 0, v_y > 0$$

$$\Delta f^{-+} = \frac{q\tau E_z}{m_{eff}} \frac{\partial f_0}{\partial v_z} \left(1 - e^{-\frac{\min(\frac{x-a}{v_x}, \frac{y}{v_y})}{\tau}}\right) \quad \text{for } v_x < 0, v_y > 0$$

$$\Delta f^{+-} = \frac{q\tau E_z}{m_{eff}} \frac{\partial f_0}{\partial v_z} \left(1 - e^{-\frac{\min(\frac{x}{v_x}, \frac{y-a}{v_y})}{\tau}}\right) \quad \text{for } v_x > 0, v_y < 0$$

$$\Delta f^{--} = \frac{q\tau E_z}{m_{eff}} \frac{\partial f_0}{\partial v_z} \left(1 - e^{-\frac{\min(\frac{x-a}{v_x}, \frac{y-a}{v_y})}{\tau}}\right) \quad \text{for } v_x < 0, v_y < 0 \quad (11)$$

Here, the first and the second signs on the subscript of Δf represent the direction of x - and y - components of the electron velocity (v_x and v_y), respectively. Using (11) in (2) and following the process as for the thin wires, the authors¹³ obtain the expression for the conductivity averaged over the cross-sectional area as

$$\sigma = \frac{1}{a^2 E_z} \int_0^a \int_0^a J_z(x, y) dx dy = \sigma_0 \left[1 - \frac{2 \int_{v_x > 0, v_y > 0} v_z^2 \{c_1 + c_2 e^{-\frac{a}{\tau v_y}}\} d\vec{v}}{\int_{v_x > 0, v_y > 0} v_z^2 d\vec{v}} \right] \quad (12)$$

where

$$c_1 = \frac{\tau v_x}{a} + \frac{\tau v_y}{a} - 2 \frac{\tau v_x \tau v_y}{a} \quad (13)$$

$$c_2 = \frac{\tau v_x}{a} - \frac{\tau v_y}{a} + 2 \frac{\tau v_x \tau v_y}{a}$$

Similar to Ref. 21, the authors¹³ derive simplified expressions for various limiting cases (e.g. $a \gg \lambda_0$, $a \ll \lambda_0$, $a \sim \lambda_0$ etc.), which form the basis of surface scattering models in various subsequent works^{16,17,25,26}. Some works have also derived simplified expressions for wires with rectangular and circular cross-sections²⁶⁻²⁸.

B. Spatial Dependence of Conductivity: An Empirical Model

The early fundamental studies of metal conductivity mainly focused on understanding the average behavior of the metal, and hence, the spatial dependence of conductivity was not

> REPLACE THIS LINE WITH YOUR MANUSCRIPT ID NUMBER (DOUBLE-CLICK HERE TO EDIT) <

widely considered. Traditionally, researchers focused on thin film and rectangular wire resistivity without the liner and barrier layers. However, in modern chips, the inclusion of barrier/liner layers in the interconnect structure makes the current transport (especially through the vias) somewhat non-trivial (as discussed before). Despite this, many of the recent works^{16–18} have used the simplified expressions derived from the FS model and utilized fitting parameters to show good match with the experiments. However, one recent work²³ does consider the spatial dependency of the conductivity by modeling the surface scattering effects using an empirical expression. Here, we briefly review some key attributes of this approach.

The resistivity model proposed²³ shown below employs two terms: the first capturing bulk resistivity and other scattering mechanisms (such as grain boundary scattering) in a lumped parameter ρ_0 , and the second accounting for spatial dependence of resistivity due to surface scattering.

$$\rho(x, y) = \rho_0 + \rho_q \left(\frac{\cosh\left[\frac{x}{\lambda_q}\right]}{\cosh\left[\frac{a}{2\lambda_q}\right]} + \frac{\cosh\left[\frac{y}{\lambda_q}\right]}{\cosh\left[\frac{b}{2\lambda_q}\right]} \right) \quad (14)$$

Here, ρ_q and λ_q are fitting parameters, and a and b are the width and height of the wire cross-section (along the x - and y -directions), respectively. The analysis²³ shows good match of the average conductivity (obtained by averaging (14) across the cross-section) with the experiments. The main merit of this approach (referred to as the ‘‘cosh’’ model subsequently) is its spatial resolution of resistivity. Using this model, the effect of barrier/liner layers and taper angles can be seamlessly integrated, as in Ref. 18. However, this method does not directly capture the relationship of the conductivity with the physical parameters (such as p , λ_0 etc.).

To address the limitations of the current models, in this paper, we derive the spatial dependence of the conductivity using the FS theory, thereby developing a model that is capable of predicting the relationship of the spatially resolved conductivity with the physical parameters.

III. SPATIALLY RESOLVED FS (SRFS) MODEL FOR RECTANGULAR WIRES

In this section, we present the derivation of the space-dependence of the surface scattering model for rectangular wires following the FS approach, which we refer to as the spatially resolved FS or SRFS model. We start with purely diffusive scatter i.e. specularity (p)=0. We then generalize the discussion for an arbitrary p (between 0 and 1). We assume that the electric field and the current flow is along the z -direction, and the wire has width and height equal to a and b (along the x - and y -directions), respectively – Fig. 3. For all the discussions in this paper, we assume the origin of the coordinate system to be in the lower left corner of the wire cross-section. (Later on in the paper, we shift the origin following the symmetry - more on that later).

A. Purely Diffusive Surface Scattering ($p=0$)

Following the same approach as discussed in Section II A for a square wire and accounting for scattering at the four surfaces of the wire, Δf for a rectangular wire is obtained as

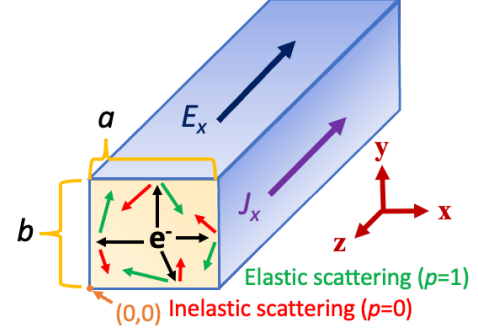


Fig. 3. Rectangular wire structure used for modeling showing fully elastic (specularity $p=1$) or inelastic scattering ($p=0$) when electron hits the four surfaces.

$$\begin{aligned} \Delta f^{++} &= \frac{q\tau E_z}{m_{eff}} \frac{\partial f_0}{\partial v_z} \left(1 - e^{-\frac{\min\left(\frac{x}{v_x}, \frac{y}{v_y}\right)}{\tau}} \right) & \text{for } v_x > 0, v_y > 0 \\ \Delta f^{-+} &= \frac{q\tau E_z}{m_{eff}} \frac{\partial f_0}{\partial v_z} \left(1 - e^{-\frac{\min\left(\frac{x-a}{v_x}, \frac{y}{v_y}\right)}{\tau}} \right) & \text{for } v_x < 0, v_y > 0 \\ \Delta f^{+-} &= \frac{q\tau E_z}{m_{eff}} \frac{\partial f_0}{\partial v_z} \left(1 - e^{-\frac{\min\left(\frac{x}{v_x}, \frac{y-b}{v_y}\right)}{\tau}} \right) & \text{for } v_x > 0, v_y < 0 \\ \Delta f^{--} &= \frac{q\tau E_z}{m_{eff}} \frac{\partial f_0}{\partial v_z} \left(1 - e^{-\frac{\min\left(\frac{x-a}{v_x}, \frac{y-b}{v_y}\right)}{\tau}} \right) & \text{for } v_x < 0, v_y < 0 \end{aligned} \quad (15)$$

In order to retain the spatial dependency of the conductivity, the current density ($J_z(x, y)$) needs to be divided by E_z without averaging along the width and height directions. Thus, spatially-resolved conductivity ($\sigma(x, y)$) accounting for surface scattering can be obtained.

$$\begin{aligned} \sigma(x, y) &= -\frac{2q^2 m_{eff}^2}{h^3} \int \frac{\partial f_0}{\partial v} \frac{v_z \tau}{v} \zeta \left(\frac{x}{\tau v_x}, \frac{y}{\tau v_y} \right) dv_x dv_y dv_z \quad (16) \end{aligned}$$

Here ζ is a function that depends on the spatial location (x and y) and the electron velocities v_x and v_y and is derived by substituting the four Δf functions of (15) in the expression for J in (2). We will derive the explicit form of this function subsequently.

Transforming the electron velocities to the spherical coordinate system, and following the FS approach (i.e. utilizing the degenerate electron gas condition in (5) and substituting the electron mean free path (λ_0) from (6)), we obtain $\sigma(x, y)$ as

$$\begin{aligned} \sigma(x, y) &= -\frac{2q^2 m_{eff}^2}{h^3} \int_{\theta=0}^{\pi} \int_{\Phi=0}^{2\pi} \tau \tilde{v}^3 \cos^2 \theta \sin \theta \\ &\times \zeta \left(\frac{x}{\lambda_0 \sin \theta \cos \Phi}, \frac{y}{\lambda_0 \sin \theta \sin \Phi} \right) d\Phi d\theta \quad (17) \end{aligned}$$

By substituting bulk conductivity (σ_0) from (8) in (17), we obtain

$$\begin{aligned} \sigma(x, y) &= \frac{3}{4} \sigma_0 \int_{\theta=0}^{\pi} \int_{\Phi=0}^{2\pi} \zeta \left(\frac{x}{\lambda_0 \sin \theta \cos \Phi}, \frac{y}{\lambda_0 \sin \theta \sin \Phi} \right) \cos^2 \theta \sin \theta d\Phi d\theta \quad (18) \end{aligned}$$

> REPLACE THIS LINE WITH YOUR MANUSCRIPT ID NUMBER (DOUBLE-CLICK HERE TO EDIT) <

To simplify the ζ function, we consider four cases based on the signs of v_x and v_y (similar to (15)): (i) $v_x > 0, v_y > 0$, for which $\Phi = 0 \rightarrow \frac{\pi}{2}$, and $\Delta f = \Delta f^{++}$, (ii) $v_x < 0, v_y > 0$, ($\Phi = \frac{\pi}{2} \rightarrow \pi$, and $\Delta f = \Delta f^{-+}$), (iii) $v_x > 0, v_y < 0$, ($\Phi = \pi \rightarrow \frac{3\pi}{2}$, and $\Delta f = \Delta f^{+-}$), and (iv) $v_x < 0, v_y < 0$, ($\Phi = \frac{3\pi}{2} \rightarrow 2\pi$, and $\Delta f = \Delta f^{--}$). Thus, the integral of ζ with respect to Φ can be written as

$$\begin{aligned} & \int_{\Phi=0}^{2\pi} \zeta \left(\frac{x}{\lambda_0 \sin\theta \cos\Phi}, \frac{y}{\lambda_0 \sin\theta \sin\Phi} \right) d\Phi \\ &= \int_{\Phi=0}^{\frac{\pi}{2}} \zeta(\Phi)|_{\Delta f = \Delta f^{++}} d\Phi + \int_{\Phi=\frac{\pi}{2}}^{\pi} \zeta(\Phi)|_{\Delta f = \Delta f^{-+}} d\Phi \quad (19) \\ &+ \int_{\Phi=\pi}^{\frac{3\pi}{2}} \zeta(\Phi)|_{\Delta f = \Delta f^{+-}} d\Phi + \int_{\Phi=\frac{3\pi}{2}}^{2\pi} \zeta(\Phi)|_{\Delta f = \Delta f^{--}} d\Phi \end{aligned}$$

We define the four integrals of the right hand side of (19) as $\eta^{++}, \eta^{-+}, \eta^{+-}, \eta^{--}$, respectively, and the left hand side of (19) as η . Thus,

$$\sigma(x, y) = \frac{3}{4} \sigma_0 \int_{\theta=0}^{\pi} \eta(x, y, \theta) \cos^2 \theta \sin \theta d\theta \quad (20)$$

where $\eta(x, y, \theta) = \eta^{++} + \eta^{-+} + \eta^{+-} + \eta^{--}$

Let us first look at η^{++} , it can be observed that the *min* function in (15) dictates that if $\frac{v_y}{v_x} = \frac{v \sin\theta \sin\Phi}{v \sin\theta \cos\Phi} = \tan\Phi < \frac{y}{x}$, Δf^{++} in (15) uses $\left(1 - e^{-\frac{x}{\lambda_0 \sin\theta \cos\Phi}}\right)$, else it uses $\left(1 - e^{-\frac{y}{\lambda_0 \sin\theta \sin\Phi}}\right)$. Thus,

$$\begin{aligned} \eta^{++} &= \int_0^{\tan^{-1}\left(\frac{y}{x}\right)} \left(1 - e^{-\frac{x}{\lambda_0 \sin\theta \cos\Phi}}\right) d\Phi \\ &+ \int_{\tan^{-1}\left(\frac{y}{x}\right)}^{\frac{\pi}{2}} \left(1 - e^{-\frac{y}{\lambda_0 \sin\theta \sin\Phi}}\right) d\Phi \quad (21a) \end{aligned}$$

In a similar manner, when we repeat this for other η functions and change the limits of integration to $0 \rightarrow \frac{\pi}{2}$, we get the following expressions.

$$\begin{aligned} \eta^{-+} &= \int_0^{\tan^{-1}\left(\frac{y}{a-x}\right)} \left(1 - e^{-\frac{a-x}{\lambda_0 \sin\theta \cos\Phi}}\right) d\Phi \\ &+ \int_{\tan^{-1}\left(\frac{y}{a-x}\right)}^{\frac{\pi}{2}} \left(1 - e^{-\frac{y}{\lambda_0 \sin\theta \sin\Phi}}\right) d\Phi \quad (21b) \end{aligned}$$

$$\begin{aligned} \eta^{+-} &= \int_0^{\tan^{-1}\left(\frac{b-y}{x}\right)} \left(1 - e^{-\frac{x}{\lambda_0 \sin\theta \cos\Phi}}\right) d\Phi \\ &+ \int_{\tan^{-1}\left(\frac{b-y}{x}\right)}^{\frac{\pi}{2}} \left(1 - e^{-\frac{b-y}{\lambda_0 \sin\theta \sin\Phi}}\right) d\Phi \quad (21c) \end{aligned}$$

$$\begin{aligned} \eta^{--} &= \int_0^{\tan^{-1}\left(\frac{b-y}{a-x}\right)} \left(1 - e^{-\frac{a-x}{\lambda_0 \sin\theta \cos\Phi}}\right) d\Phi \\ &+ \int_{\tan^{-1}\left(\frac{b-y}{a-x}\right)}^{\frac{\pi}{2}} \left(1 - e^{-\frac{b-y}{\lambda_0 \sin\theta \sin\Phi}}\right) d\Phi \quad (21d) \end{aligned}$$

Substituting (20) in (19), we can rewrite the expression for η as

$$\begin{aligned} \eta(x, y, \theta) &= \sum_{n,d} \left[\int_0^{\tan^{-1}\left(\frac{n}{d}\right)} \left(1 - e^{-\frac{d}{\lambda_0 \sin\theta \cos\Phi}}\right) d\Phi \right. \\ &\left. + \int_{\tan^{-1}\left(\frac{n}{d}\right)}^{\frac{\pi}{2}} \left(1 - e^{-\frac{n}{\lambda_0 \sin\theta \sin\Phi}}\right) d\Phi \right] \quad (22) \end{aligned}$$

where $(n, d) \rightarrow \{(y, x), (y, a-x), (b-y, x), (b-y, a-x)\}$.

Let us call these four points as the boundary points. Depending on the spatial location, the ascending order of the four boundary points from 0 to $\frac{\pi}{2}$ can have eight different combinations (shown in the Appendix A1). In general, the order of the boundary points may be needed to solve (22), which, being space-dependent, may make the expressions complicated. However, we solve (22) following an approach which makes the order of the breaking points irrelevant and thus considerably simplifies the final SRFS conductivity model. The details of our approach are provided in Appendix A1.

Substituting the simplified expression of (22) in (20), we obtained the final space-dependent conductivity as

$$\sigma(x, y) = \frac{3}{4} \sigma_0 \int_{\theta=0}^{\pi} \eta(x, y, \theta) \cos^2 \theta \sin \theta d\theta \quad (23)$$

$$\begin{aligned} \eta(x, y, \theta) &= 2\pi \\ &- 2 \int_{\Phi=0}^{\frac{\pi}{2}} \left\{ e^{-\frac{b}{2\lambda_0 \sin\theta \sin\Phi}} \cosh\left(\frac{y - \frac{b}{2}}{\lambda_0 \sin\theta \sin\Phi}\right) \right. \\ &+ \left. e^{-\frac{a}{2\lambda_0 \sin\theta \cos\Phi}} \cosh\left(\frac{x - \frac{a}{2}}{\lambda_0 \sin\theta \cos\Phi}\right) \right\} d\Phi \quad (24) \\ &- \frac{1}{2} \sum_{n,d} \int_{\Phi=0}^{\frac{\pi}{2}} \left| e^{-\frac{d}{\lambda_0 \sin\theta \cos\Phi}} - e^{-\frac{n}{\lambda_0 \sin\theta \sin\Phi}} \right| d\Phi \end{aligned}$$

where $(n, d) \rightarrow \{(y, x), (y, a-x), (b-y, x), (b-y, a-x)\}$ and $x \in [0, a]$, $y \in [0, b]$

B. Specular Surface Scattering (General p)

Let us now generalize the SRFS model accounting for specularity (p) at the surfaces (which, as may be recalled, models both diffusive (inelastic) and elastic scattering at the surface). Here, we consider that all the four surfaces have the same value of p .

As noted earlier, the exact solution for general p is challenging to obtain for square/rectangular wires²⁰ (although for thin films and circular cross-sections, the exact solutions have been obtained^{13,14}). Therefore, here, we propose approximate expressions for Δf and follow the approach we discussed in the previous sub-section to obtain the spatially resolved conductivity. The approximate expression for Δf are given below.

$$\begin{aligned} \Delta f^{++} &= \frac{q\tau E_z}{m_{eff}} \frac{\partial f_0}{\partial v_z} \left(1 - (1-p) \times \max \left\{ \frac{e^{-\frac{x}{\tau v_x}}}{1-p e^{-a/\tau v_x}}, \frac{e^{-\frac{y}{\tau v_y}}}{1-p e^{-a/\tau v_y}} \right\} \right) \\ &\quad \text{for } v_x > 0, v_y > 0 \\ \Delta f^{-+} &= \frac{q\tau E_z}{m_{eff}} \frac{\partial f_0}{\partial v_z} \left(1 - (1-p) \times \max \left\{ \frac{e^{-\frac{x-a}{\tau v_x}}}{1-p e^{a/\tau v_x}}, \frac{e^{-\frac{y}{\tau v_y}}}{1-p e^{-a/\tau v_y}} \right\} \right) \end{aligned}$$

> REPLACE THIS LINE WITH YOUR MANUSCRIPT ID NUMBER (DOUBLE-CLICK HERE TO EDIT) <

$$\Delta f^{+-} = \frac{q\tau E_z}{m_{eff}} \frac{\partial f_0}{\partial v_z} \left(1 - (1-p) \times \max \left\{ \frac{e^{-\frac{x}{\tau v_x}}}{1 - p e^{-a/\tau v_x}}, \frac{e^{-\frac{y-b}{\tau v_y}}}{1 - p e^{a/\tau v_y}} \right\} \right)$$

for $v_x < 0, v_y > 0$

$$\Delta f^{--} = \frac{q\tau E_z}{m_{eff}} \frac{\partial f_0}{\partial v_z} \left(1 - (1-p) \times \max \left\{ \frac{e^{-\frac{x-a}{\tau v_x}}}{1 - p e^{a/\tau v_x}}, \frac{e^{-\frac{y-b}{\tau v_y}}}{1 - p e^{a/\tau v_y}} \right\} \right)$$

for $v_x > 0, v_y < 0$

$$\Delta f^{--} = \frac{q\tau E_z}{m_{eff}} \frac{\partial f_0}{\partial v_z} \left(1 - (1-p) \times \max \left\{ \frac{e^{-\frac{x-a}{\tau v_x}}}{1 - p e^{a/\tau v_x}}, \frac{e^{-\frac{y-b}{\tau v_y}}}{1 - p e^{a/\tau v_y}} \right\} \right)$$

for $v_x < 0, v_y < 0$

(25)

The choice of the approximations are based on the following observations and conditions. First, the solution obtained from the SRFS model is exact for $p=0$, while for $p=1$ the solution is trivial (i.e. spatially uniform conductivity = bulk conductivity). Thus, for general p , the solution should lie somewhere in between these two exact extreme solutions. Also, the approximate expressions should converge to the exact solution for $p=0$ and $p=1$. (Note, substituting $p=0$ in (25) yields (15) with the *max* function in (25) translating to the *min* of the argument of the exponential function in (15)). Second, the proposed solution should converge to the exact solution for the thin wire (i.e. when one of the dimension a or b is infinitely large). Third, the expressions should be such that they can be seamlessly applied to the method of spatial resolution that we have discussed in the previous section. The expressions in (25) satisfy these requirements. These models are approximate because they neglect interactions between specular scattering from orthogonal surfaces. To consider complete scattering interactions in rectangular surfaces, further refinements to (25) are needed. In this paper, we proceed with the expressions in (25) and derive the spatially resolved conductivity for general p . Later, we will show how good these approximations by comparing the average conductivity to the previous works^{19,24}.

Following the same process as described in the previous subsection for $p=0$, we obtain the final SRFS conductivity model as a function of specularity (p) as

$$\sigma(x, y) = \frac{3}{4} \sigma_0 \int_{\theta=0}^{\pi} \eta(x, y, \theta) \cos^2 \theta \sin \theta d\theta \quad (26)$$

$$\eta(x, y, \theta) = 2\pi - (1-p) \times \left[2 \int_{\Phi=0}^{\frac{\pi}{2}} \frac{e^{-\frac{a}{2\lambda_0 \sin \theta \cos \Phi}} \times \cosh \left(\frac{x - \frac{a}{2}}{\lambda_0 \sin \theta \cos \Phi} \right)}{1 - p e^{-\frac{a}{\lambda_0 \sin \theta \cos \Phi}}} d\Phi \right. \\ \left. + 2 \int_{\Phi=0}^{\frac{\pi}{2}} \frac{e^{-\frac{b}{2\lambda_0 \sin \theta \sin \Phi}} \times \cosh \left(\frac{y - \frac{b}{2}}{\lambda_0 \sin \theta \sin \Phi} \right)}{1 - p e^{-\frac{b}{\lambda_0 \sin \theta \sin \Phi}}} d\Phi \right. \\ \left. + \frac{1}{2} \sum_{n,d} \int_0^{\frac{\pi}{2}} \left| \frac{e^{-\frac{d}{\lambda_0 \sin \theta \cos \Phi}}}{1 - p e^{-\frac{a}{2\lambda_0 \sin \theta \cos \Phi}}} - \frac{e^{-\frac{n}{\lambda_0 \sin \theta \sin \Phi}}}{1 - p e^{-\frac{b}{2\lambda_0 \sin \theta \sin \Phi}}} \right| d\Phi \right] \quad (27)$$

where $(n, d) \rightarrow \{(y, x), (y, a-x), (b-y, x), (b-y, a-x)\}$ and $x \in [0, a], y \in [0, b]$

The first term in (27) corresponds to the bulk conductivity and the rest of the terms to surface scattering. Separating the two components, we can write

$$\sigma(x, y) = \sigma_0 - \sigma_{SR}(x, y) \\ = \sigma_0 - \frac{3}{4} \sigma_0 \int_{\theta=0}^{\pi} \Delta \eta(x, y, \theta) \cos^2 \theta \sin \theta d\theta \quad (28)$$

$$\Delta \eta(x, y, \theta) = (1-p) \times \left[2 \int_{\Phi=0}^{\frac{\pi}{2}} \frac{e^{-\frac{a}{2\lambda_0 \sin \theta \cos \Phi}} \times \cosh \left(\frac{x - \frac{a}{2}}{\lambda_0 \sin \theta \cos \Phi} \right)}{1 - p e^{-\frac{a}{2\lambda_0 \sin \theta \cos \Phi}}} d\Phi \right. \\ \left. + 2 \int_{\Phi=0}^{\frac{\pi}{2}} \frac{e^{-\frac{b}{2\lambda_0 \sin \theta \sin \Phi}} \times \cosh \left(\frac{y - \frac{b}{2}}{\lambda_0 \sin \theta \sin \Phi} \right)}{1 - p e^{-\frac{b}{2\lambda_0 \sin \theta \sin \Phi}}} d\Phi \right. \\ \left. + \frac{1}{2} \sum_{n,d} \int_0^{\frac{\pi}{2}} \left| \frac{e^{-\frac{d}{\lambda_0 \sin \theta \cos \Phi}}}{1 - p e^{-\frac{a}{2\lambda_0 \sin \theta \cos \Phi}}} - \frac{e^{-\frac{n}{\lambda_0 \sin \theta \sin \Phi}}}{1 - p e^{-\frac{b}{2\lambda_0 \sin \theta \sin \Phi}}} \right| d\Phi \right] \quad (29)$$

where $(n, d) \rightarrow \{(y, x), (y, a-x), (b-y, x), (b-y, a-x)\}$ and $x \in [0, a], y \in [0, b]$

Note in (27), the conductivity components (i.e. bulk (σ_0) and surface scattering (σ_{SR})) are subtracted to obtain the overall conductivity. This is different from some recent empirical works²³ which add the resistivity components rather than subtract the conductivity components. Since the conductivity component subtraction follows from the rigorous FS treatment, that should be a preferred method to combine different mechanisms as opposed to resistivity addition.

As can be observed from (27) and (29), the SRFS model offers (1) the space-dependence of conductivity as well as (2) its explicit relationship to physical parameters p, λ_0 and the wire cross-section width (a) and height (b).

C. Normalization and Origin Shifting

Before we conclude this section, we present a variation of the SRFS model by normalizing the parameters and shifting the origin of the coordinate system.

First, we shift the origin of the coordinate system to the center of the wire (rather than the corner, as done in the previous sub-sections). Thus, the wire cross sectional width is from $-a/2$ to $+a/2$ and its height is from $-b/2$ to $+b/2$. Second, we follow a common practice used to express the FS model in terms of the ratio of the wire width/height and the electron mean free path²¹. For that, we define $\kappa_a = \frac{a}{\lambda_0}$ and $\kappa_b = \frac{b}{\lambda_0}$. We also normalize x and y as $x_n = \frac{x}{a/2}$ and $y_n = \frac{y}{b/2}$. Hence, x_n and y_n range from -

> REPLACE THIS LINE WITH YOUR MANUSCRIPT ID NUMBER (DOUBLE-CLICK HERE TO EDIT) <

Final SRFS model for conductivity accounting for specular surface scattering (the figure of wire schematic along with the coordinate system shown alongside)

$$\frac{\sigma_{SRFS}(x_n, y_n)}{\sigma_0} = \frac{3}{4} \int_{\theta=0}^{\pi} \eta(x_n, y_n, \theta) * \cos^2 \theta \sin \theta d\theta$$

$$\eta(x_n, y_n, \theta) = 2\pi - (1-p) \times \left[2 \int_{\Phi=0}^{\frac{\pi}{2}} \left(\frac{e^{\frac{-\kappa_a}{2\sin\theta\cos\Phi}} \times \cosh\left(\frac{\kappa_a \times x_n}{2\sin\theta\cos\Phi}\right)}{1 - p e^{\frac{-\kappa_a}{\sin\theta\cos\Phi}}} + \frac{e^{\frac{-\kappa_b}{2\sin\theta\sin\Phi}} \times \cosh\left(\frac{\kappa_b \times y_n}{2\sin\theta\sin\Phi}\right)}{1 - p * e^{\frac{-\kappa_b}{\sin\theta\sin\Phi}}}\right) d\Phi \right. \\ \left. + \frac{1}{2} \sum_{n,d} \int_{\Phi=0}^{\frac{\pi}{2}} \left| \frac{e^{\frac{-\kappa_a \times d}{2 * \sin\theta\cos\Phi}}}{1 - p e^{\frac{-\kappa_a}{\sin\theta\cos\Phi}}} - \frac{e^{\frac{-\kappa_b \times n}{2 * \sin\theta\sin\Phi}}}{1 - p * e^{\frac{-\kappa_b}{\sin\theta\sin\Phi}}} \right| d\Phi \right]$$

$$\frac{\sigma_{SRFS}(x_n, y_n)}{\sigma_0} = 1 - \frac{\sigma_{SR}(x_n, y_n)}{\sigma_0} = 1 - \frac{3}{4} \int_{\theta=0}^{\pi} \Delta\eta(x, y, \theta) \cos^2 \theta \sin \theta d\theta$$

$$\Delta\eta(x_n, y_n, \theta) = (1-p) \times \left[2 \int_{\Phi=0}^{\frac{\pi}{2}} \left(\frac{e^{\frac{-\kappa_a}{2\sin\theta\cos\Phi}} \times \cosh\left(\frac{\kappa_a \times x_n}{2\sin\theta\cos\Phi}\right)}{1 - p e^{\frac{-\kappa_a}{\sin\theta\cos\Phi}}} + \frac{e^{\frac{-\kappa_b}{2\sin\theta\sin\Phi}} \times \cosh\left(\frac{\kappa_b \times y_n}{2\sin\theta\sin\Phi}\right)}{1 - p e^{\frac{-\kappa_b}{\sin\theta\sin\Phi}}}\right) d\Phi \right. \\ \left. + \frac{1}{2} \sum_{n,d} \int_{\Phi=0}^{\frac{\pi}{2}} \left| \frac{e^{\frac{-\kappa_a \times d}{2 * \sin\theta\cos\Phi}}}{1 - p e^{\frac{-\kappa_a}{\sin\theta\cos\Phi}}} - \frac{e^{\frac{-\kappa_b \times n}{2 * \sin\theta\sin\Phi}}}{1 - p * e^{\frac{-\kappa_b}{\sin\theta\sin\Phi}}} \right| d\Phi \right]$$

where $(n, d) \rightarrow \{(1 + y_n, 1 + x_n), (1 - y_n, 1 + x_n), (1 + y_n, 1 - x_n), (1 - y_n, 1 - x_n)\}$

$$x_n = \frac{x}{a/2} \in [-1, 1], \quad y_n \in \frac{y}{b/2} [-1, 1]; \quad \kappa_a = \frac{a}{\lambda_0}, \quad \kappa_b = \frac{b}{\lambda_0}$$

1 to 1. With this, the final expressions for SRFS conductivity are summarized in the top of this page. (It may be noted that when implementing this in software like MATLAB, it is recommended to replace *cosh* with its exponential-based representation and combine it with the exponential preceding it).

The expression obtained is generic and can be applied for thin films (of thickness b along the along the y -direction) by setting $\kappa_a \rightarrow \infty$. The model for a thin film simplifies to

$$\frac{\sigma_{SRFS}(y_n)}{\sigma_0} = \frac{3}{4} \int_{\theta=0}^{\pi} \eta(y_n, \theta) * \cos^2 \theta \sin \theta d\theta$$

$$\eta(y_n, \theta) = 2\pi - (1-p) \times 4 \int_{\Phi=0}^{\frac{\pi}{2}} \left(\frac{e^{\frac{-\kappa_b}{2\sin\theta\sin\Phi}} \times \cosh\left(\frac{\kappa_b \times y_n}{2\sin\theta\sin\Phi}\right)}{1 - p * e^{\frac{-\kappa_b}{\sin\theta\sin\Phi}}}\right) d\Phi \quad (30)$$

where $y_n \in \frac{y}{b/2} [-1, 1]$ and $\kappa_b = \frac{b}{\lambda_0}$

IV. ANALYSIS

A. Proposed SRFS Model and Previous FS-based Models

As mentioned before, the previous works based on FS models have utilized the simplified versions of (12) derived in Ref. 13 to model the effect of surface scattering on the conductivity of square wires. Here, we utilize the models¹³ (provided for the reader in the appendix A2) and compare them to the values obtained by averaging the SRFS models across the cross section to validate our approach. The comparison is shown in Fig. 4 illustrating how conductivity increases with

increasing κ . In Ref. 13, the expressions assume that all electrons experience inelastic surface scattering ($p=0$). It can be observed in Fig. 4 that the average SRFS model for $p=0$ overlaps with the values in Ref. 13, validating the expressions presented in the previous sections. We also show conductivity versus κ for other values of p . As p increases and electrons experience more elastic scattering, the conductivity rises sharply. For large p and large κ , the conductivity is close to the bulk value, as expected.

We also compare the FS model with the average conductivity obtained from the proposed SRFS model for a thin film in Fig. 5. The scatter points are obtained from Ref. 21 for p equals to 0 and 0.5. Since our SRFS model is general, we set κ_a to be very large value to simulate a thin film and study the effect of different κ_b . Our SRFS model results matches the results from

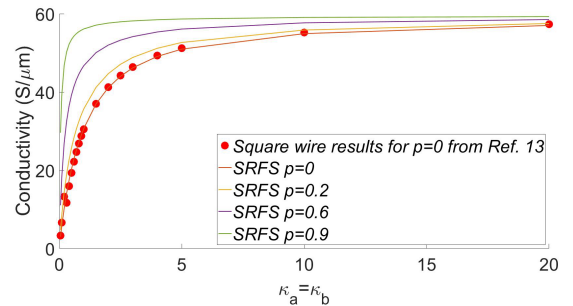
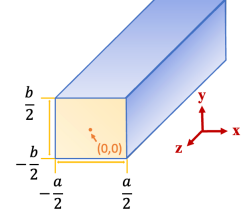


Fig. 4. Conductivity vs κ for different specularity p for a square wire showing the comparison between the proposed SRFS model with the results¹³.

> REPLACE THIS LINE WITH YOUR MANUSCRIPT ID NUMBER (DOUBLE-CLICK HERE TO EDIT) <

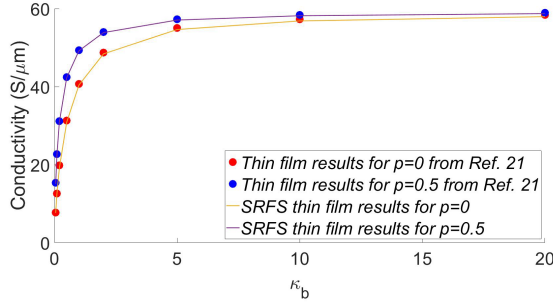


Fig. 5. Conductivity vs κ for different specularity p for a thin film showing the comparison between the proposed SRFS model with the results²¹.

the original FS model²¹ for both p values and wide range of dimensions, which again validates the SRFS model.

B. Proposed SRFS Model and Kinetic Theory-based Model for Specular Surface Scattering in Square Interconnects

As noted before, the work¹⁹ proposes an infinite summation series to model the conductivity averaged across the cross-section considering specular surface scattering for rectangular interconnects, as given below:

$$\left(\frac{\sigma}{\sigma_0}\right)_{p,\lambda_0} = (1-p)^2 \sum_{j=1}^{\infty} \left\{ j p^{j-1} \left(\frac{\sigma}{\sigma_0}\right)_{p=0,\lambda_0/j} \right\} \quad (31)$$

Where the $\frac{\sigma}{\sigma_0}$ ratio for general p is define as the infinite weighted sum of $\frac{\sigma}{\sigma_0}$ for $p=0$ and $\lambda_0 = \lambda_0/j$. We implement (31) by substituting the average conductivity obtained from our SRFS model for $p=0$ (which, recall, is exact) into the terms

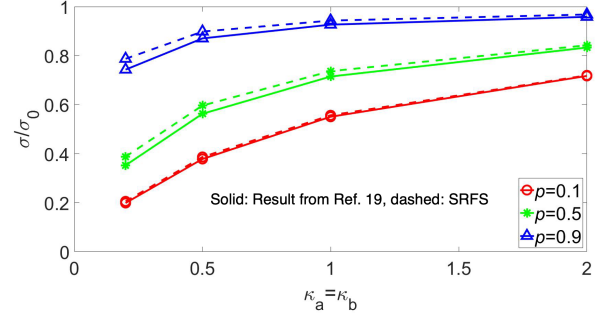


Fig. 6. σ/σ_0 (conductivity normalized to bulk conductivity) for different κ and p for a square wire between the approximation proposed¹⁹ and SRFS, showing SRFS model is able to capture conductivity for general p .

$\left(\frac{\sigma}{\sigma_0}\right)_{p=0,\lambda_0/j}$. We compare the results obtained from this approach to the average conductivity obtained from the proposed SRFS model for general p (see Fig. 6). At small p , our SRFS model shows < 3% difference compared to (31). The maximum difference is < 10% when $p=0.5$. When p increases further, the difference reduced again to < 6% @ $p=0.9$. Thus, the proposed SRFS approach is able to model the conductivity for general specularity (p) in rectangular interconnects with a reasonable accuracy. While the proposed SRFS approach needs to compute the complex integrals only once, the technique from Ref. 19 involving infinite sum in (31) needs computation of the complex integrals many times (depending on the maximum value of j).

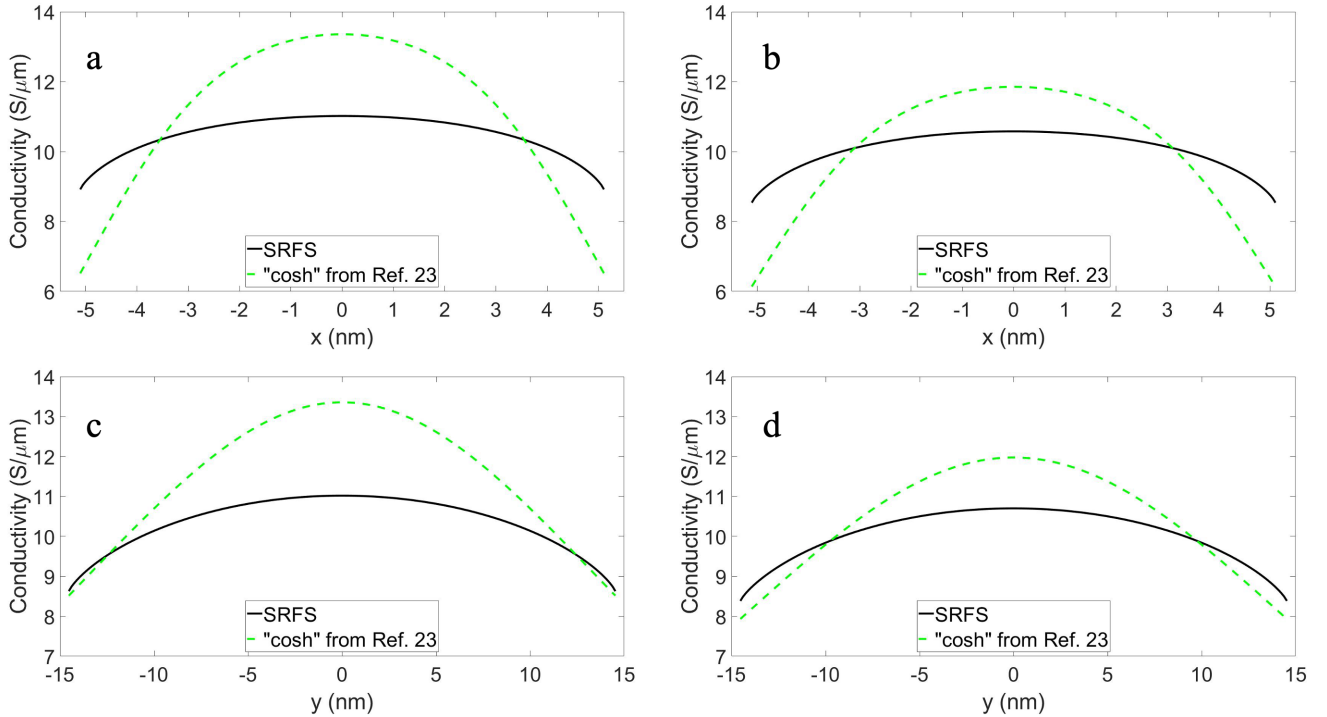


Fig. 7. Conductivity comparison between the proposed SRFS model with “cosh” model along x direction for a) $y=0$ b) $y=7.25$ nm, along y direction for c) $x=0$ d) $x=2.5$ nm, highlighting the mismatch between the proposed physical model and an empirical approach.

> REPLACE THIS LINE WITH YOUR MANUSCRIPT ID NUMBER (DOUBLE-CLICK HERE TO EDIT) <

C. Proposed SRFS Model versus “cosh” Model

The “cosh” model²³ is another spatially resolved conductivity model which uses fitting parameters to match the average conductivity values obtained from the experiment, as described before. Here, we compare the spatial dependence of conductivity predicted by the proposed SRFS model with the “cosh” model. We use width of 10nm and thickness of 29nm for the interconnect as used²³. Further, following the method²³, we lump the bulk conductivity and the grain boundary scattering component in the first term of (28) in the SRFS model, and use the same value of this lumped parameter as in Ref. 23. We then match the average conductivity from SRFS model to the “cosh” model by sweeping p . Specifically, the “cosh” model reports an average conductivity of $9.8 \text{ S}/\mu\text{m}$. We found $p=0.663$ in the SRFS model yielding the same value.

After matching the average conductivity, we compare the spatial dependence of conductivity obtained from the two models. The conductivity along the width (x) direction for $y=0$ and $y=7.25\text{nm}$ are plotted in Fig. 7a and 7b, showing a large mismatch between the physical (SRFS) and the empirical (“cosh”) approaches. Similar mismatches are observed for the conductivity along y in Fig. 7c and 7d. The SRFS model has a much flatter conductivity profile compared to the “cosh” model. Although the average conductivity is the same between the two models, the spatial-dependence of conductivity due to surface scattering shows a significant difference, highlighting the importance for a physics-based spatially resolved conductivity model (such as proposed SRFS approach) as opposed to an empirical approach.

Since the proposed SRFS approach for a general p involves

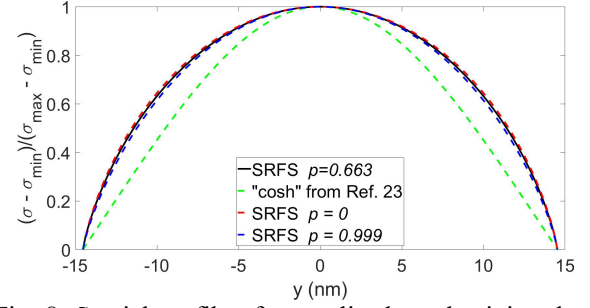


Fig. 8. Spatial profile of normalized conductivity along y direction for $x=0$, listing three different p values for SRFS and “cosh” model²³. Here, σ_{min} and σ_{max} are the minimum and maximum σ . The results show that the SRFS $p=0.663$ spatial profile lies between $p=0$ (exact) and $p \rightarrow 1$ spatial

some approximations, we show the conductivity profiles for $p=0$ (exact) and $p \rightarrow 1$ along with $p=0.663$ in Fig. 8 (along the y -axis for $x=0$). The trends illustrate the similar spatial profile for the SRFS model for different values of p . As expected, the conductivity spatial profile for $p = 0.663$ lies between the bounds i.e. $p=0$ and $p \rightarrow 1$. On the other hand, that the spatial profile from “cosh” model lies outside the bounds, suggesting that the proposed SRFS model is more accurate than this empirical approach.

D. SRFS Conductivity for Different κ and p

We show the spatial dependence of conductivity for a square wire predicted by the proposed SRFS model $\kappa=\kappa_a=\kappa_b=0.2, 1, 5$ and $p=0, 0.5, 0.9$ in Fig. 9. At lower κ values, the surface

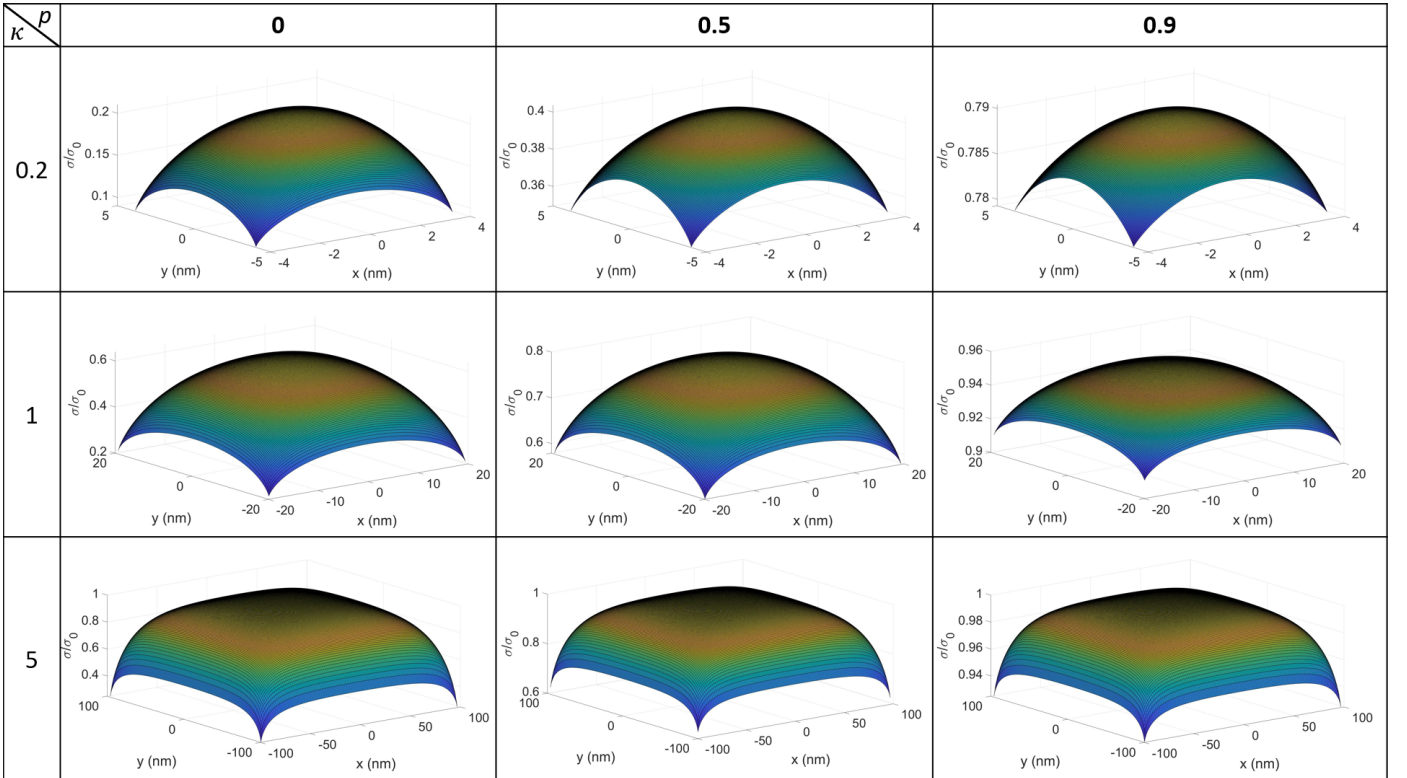


Fig. 9. The spatial profiles for σ/σ_0 (conductivity normalized to bulk conductivity) for different κ and p for a square wire, showing as p increases conductivity also increases, as κ increases conductivity increases to bulk conductivity especially at the center of the wire.

> REPLACE THIS LINE WITH YOUR MANUSCRIPT ID NUMBER (DOUBLE-CLICK HERE TO EDIT) <

scattering has a larger effect on the conductivity (compared to larger κ), thus, the conductivity is smaller at the center. For small κ , the conductivity reduces smoothly when moving towards the four edges. At larger κ , the surface scattering effect is reduced at the center, so it is closer to bulk conductivity at center. The profile is flat in the center and reduces relatively more sharply closer to the edges (than smaller κ). With an increase in p , the conductivity increases but the shape stays relatively similar.

V. CONCLUSION

We present a 2D spatially resolved FS (SRFS) model for capturing the surface scattering in interconnects with rectangular cross-sections. The primary advantage of our new model is that it offers both space dependence of conductivity and establishes a direct relationship with essential physical parameters. The proposed model is derived from the basic Boltzmann transport equation, which relates the spatially resolved conductivity to electron mean free path, specularity, and the dimensions of the conductor. The solution from SRFS is exact for $p=0$ (i.e. diffusive surface scattering). For general p ($p \neq 0$), we make certain approximations and show that the difference for average conductivity across the cross-section between proposed SRFS and previous works^{19,24} is reasonably small. When compared to the 1D²¹ and 2D FS models¹³, the proposed model shows a close match. We also show that a previously proposed empirical approach in Ref. 23 exhibits a large mismatch in the spatial profile compared to the physics-based modeling approach of SRFS (despite the same average conductivity), highlighting the importance of the latter model presented in this work.

> REPLACE THIS LINE WITH YOUR MANUSCRIPT ID NUMBER (DOUBLE-CLICK HERE TO EDIT) <

APPENDIX A1

In Section III, we discussed the boundary points that define which of the two expressions to use for the “min” function based on the x and y coordinates in (15). When we integrate (22), in general, the order of these boundary points would be needed in the range from 0 to $\frac{\pi}{2}$. If we sort in these boundary points in the ascending order, there are eight different cases depending on the location shown below

$$\begin{aligned}
 \text{I} : 0 &\rightarrow \frac{y}{a-x} \rightarrow \frac{y}{x} \rightarrow \frac{b-y}{a-x} \rightarrow \frac{b-y}{x} \rightarrow \frac{\pi}{2} \\
 \text{II} : 0 &\rightarrow \frac{y}{a-x} \rightarrow \frac{b-y}{a-x} \rightarrow \frac{y}{x} \rightarrow \frac{b-y}{x} \rightarrow \frac{\pi}{2} \\
 \text{III} : 0 &\rightarrow \frac{b-y}{a-x} \rightarrow \frac{y}{a-x} \rightarrow \frac{b-y}{a-x} \rightarrow \frac{y}{x} \rightarrow \frac{\pi}{2} \\
 \text{IV} : 0 &\rightarrow \frac{b-y}{a-x} \rightarrow \frac{b-y}{x} \rightarrow \frac{y}{a-x} \rightarrow \frac{y}{x} \rightarrow \frac{\pi}{2} \\
 \text{V} : 0 &\rightarrow \frac{b-y}{x} \rightarrow \frac{b-y}{a-x} \rightarrow \frac{y}{x} \rightarrow \frac{y}{a-x} \rightarrow \frac{\pi}{2} \\
 \text{VI} : 0 &\rightarrow \frac{b-y}{x} \rightarrow \frac{y}{x} \rightarrow \frac{b-y}{a-x} \rightarrow \frac{y}{a-x} \rightarrow \frac{\pi}{2} \\
 \text{VII} : 0 &\rightarrow \frac{y}{x} \rightarrow \frac{b-y}{x} \rightarrow \frac{y}{a-x} \rightarrow \frac{b-y}{a-x} \rightarrow \frac{\pi}{2} \\
 \text{VIII} : 0 &\rightarrow \frac{y}{x} \rightarrow \frac{y}{a-x} \rightarrow \frac{b-y}{x} \rightarrow \frac{b-y}{a-x} \rightarrow \frac{\pi}{2}
 \end{aligned}$$

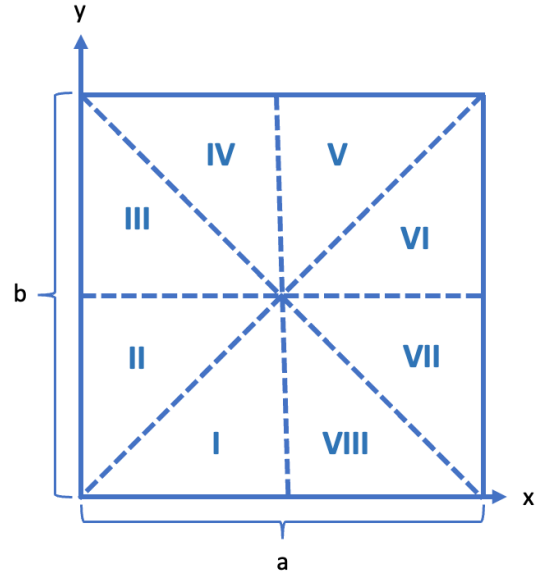


Fig. 10. Wire cross-section showing the eight regions which need to be considered for ordering the boundary points.

$$\begin{aligned}
 \eta(x, y, \theta) &= \int_{\Phi=0}^{\tan^{-1}(\frac{y}{a-x})} \left\{ \left(1 - e^{-\frac{x}{\lambda_0 \sin \theta \cos \Phi}}\right) + \left(1 - e^{-\frac{a-x}{\lambda_0 \sin \theta \cos \Phi}}\right) + \left(1 - e^{-\frac{x}{\lambda_0 \sin \theta \cos \Phi}}\right) + \left(1 - e^{-\frac{a-x}{\lambda_0 \sin \theta \cos \Phi}}\right) \right\} d\Phi \\
 &+ \int_{\tan^{-1}(\frac{y}{a-x})}^{\tan^{-1}(\frac{y}{x})} \left\{ \left(1 - e^{-\frac{x}{\lambda_0 \sin \theta \cos \Phi}}\right) + \left(1 - e^{-\frac{y}{\lambda_0 \sin \theta \sin \Phi}}\right) + \left(1 - e^{-\frac{x}{\lambda_0 \sin \theta \cos \Phi}}\right) + \left(1 - e^{-\frac{a-x}{\lambda_0 \sin \theta \cos \Phi}}\right) \right\} d\Phi \\
 &+ \int_{\tan^{-1}(\frac{y}{x})}^{\tan^{-1}(\frac{b-y}{a-x})} \left\{ \left(1 - e^{-\frac{y}{\lambda_0 \sin \theta \sin \Phi}}\right) + \left(1 - e^{-\frac{y}{\lambda_0 \sin \theta \sin \Phi}}\right) + \left(1 - e^{-\frac{x}{\lambda_0 \sin \theta \cos \Phi}}\right) + \left(1 - e^{-\frac{a-x}{\lambda_0 \sin \theta \cos \Phi}}\right) \right\} d\Phi \\
 &+ \int_{\tan^{-1}(\frac{b-y}{a-x})}^{\tan^{-1}(\frac{b-y}{x})} \left\{ \left(1 - e^{-\frac{y}{\lambda_0 \sin \theta \sin \Phi}}\right) + \left(1 - e^{-\frac{y}{\lambda_0 \sin \theta \sin \Phi}}\right) + \left(1 - e^{-\frac{x}{\lambda_0 \sin \theta \cos \Phi}}\right) + \left(1 - e^{-\frac{b-y}{\lambda_0 \sin \theta \sin \Phi}}\right) \right\} d\Phi \\
 &+ \int_{\tan^{-1}(\frac{b-y}{x})}^{\frac{\pi}{2}} \left\{ \left(1 - e^{-\frac{y}{\lambda_0 \sin \theta \sin \Phi}}\right) + \left(1 - e^{-\frac{y}{\lambda_0 \sin \theta \sin \Phi}}\right) + \left(1 - e^{-\frac{b-y}{\lambda_0 \sin \theta \sin \Phi}}\right) + \left(1 - e^{-\frac{b-y}{\lambda_0 \sin \theta \sin \Phi}}\right) \right\} d\Phi
 \end{aligned} \tag{a1}$$

Track all the cases when performing the integration would increase the complexity. To counter this, we describe our approach which averts keeping track of different regions and makes the relative order of the boundary points irrelevant. To

illustrate this approach, we take region I in Fig. 10 as an example. For region I, η function can be written as (a1)

If we observe the second and third expression from (a2), they have the same integration limits and differ from each other only

Equation (a1) can be rewritten as follows by changing the upper limits of all the integrals to $\frac{\pi}{2}$.

$$\begin{aligned}
 \eta(x, y, \theta) &= \int_{\Phi=0}^{\frac{\pi}{2}} \left\{ \left(1 - e^{-\frac{x}{\lambda_0 \sin \theta \cos \Phi}}\right) + \left(1 - e^{-\frac{a-x}{\lambda_0 \sin \theta \cos \Phi}}\right) + \left(1 - e^{-\frac{x}{\lambda_0 \sin \theta \cos \Phi}}\right) + \left(1 - e^{-\frac{a-x}{\lambda_0 \sin \theta \cos \Phi}}\right) \right\} d\Phi \\
 &- \int_{\Phi=\tan^{-1}(\frac{y}{a-x})}^{\frac{\pi}{2}} \left\{ \left(1 - e^{-\frac{x}{\lambda_0 \sin \theta \cos \Phi}}\right) + \left(1 - e^{-\frac{a-x}{\lambda_0 \sin \theta \cos \Phi}}\right) + \left(1 - e^{-\frac{x}{\lambda_0 \sin \theta \cos \Phi}}\right) + \left(1 - e^{-\frac{a-x}{\lambda_0 \sin \theta \cos \Phi}}\right) \right\} d\Phi \\
 &+ \int_{\Phi=\tan^{-1}(\frac{y}{a-x})}^{\frac{\pi}{2}} \left\{ \left(1 - e^{-\frac{x}{\lambda_0 \sin \theta \cos \Phi}}\right) + \left(1 - e^{-\frac{y}{\lambda_0 \sin \theta \sin \Phi}}\right) + \left(1 - e^{-\frac{x}{\lambda_0 \sin \theta \cos \Phi}}\right) + \left(1 - e^{-\frac{a-x}{\lambda_0 \sin \theta \cos \Phi}}\right) \right\} d\Phi \\
 &- \int_{\Phi=\tan^{-1}(\frac{y}{x})}^{\frac{\pi}{2}} \left\{ \left(1 - e^{-\frac{x}{\lambda_0 \sin \theta \cos \Phi}}\right) + \left(1 - e^{-\frac{y}{\lambda_0 \sin \theta \sin \Phi}}\right) + \left(1 - e^{-\frac{x}{\lambda_0 \sin \theta \cos \Phi}}\right) + \left(1 - e^{-\frac{a-x}{\lambda_0 \sin \theta \cos \Phi}}\right) \right\} d\Phi
 \end{aligned} \tag{a2}$$

> REPLACE THIS LINE WITH YOUR MANUSCRIPT ID NUMBER (DOUBLE-CLICK HERE TO EDIT) <

$$\begin{aligned}
& + \int_{\Phi=\tan^{-1}(\frac{y}{x})}^{\frac{\pi}{2}} \left\{ \left(1 - e^{-\frac{y}{\lambda_0 \sin \theta \sin \Phi}} \right) + \left(1 - e^{-\frac{y}{\lambda_0 \sin \theta \sin \Phi}} \right) + \left(1 - e^{-\frac{x}{\lambda_0 \sin \theta \cos \Phi}} \right) + \left(1 - e^{-\frac{a-x}{\lambda_0 \sin \theta \cos \Phi}} \right) \right\} d\Phi \\
& - \int_{\Phi=\tan^{-1}(\frac{b-y}{a-x})}^{\frac{\pi}{2}} \left\{ \left(1 - e^{-\frac{y}{\lambda_0 \sin \theta \sin \Phi}} \right) + \left(1 - e^{-\frac{y}{\lambda_0 \sin \theta \sin \Phi}} \right) + \left(1 - e^{-\frac{x}{\lambda_0 \sin \theta \cos \Phi}} \right) + \left(1 - e^{-\frac{a-x}{\lambda_0 \sin \theta \cos \Phi}} \right) \right\} d\Phi \\
& + \int_{\Phi=\tan^{-1}(\frac{b-y}{a-x})}^{\frac{\pi}{2}} \left\{ \left(1 - e^{-\frac{y}{\lambda_0 \sin \theta \sin \Phi}} \right) + \left(1 - e^{-\frac{y}{\lambda_0 \sin \theta \sin \Phi}} \right) + \left(1 - e^{-\frac{x}{\lambda_0 \sin \theta \cos \Phi}} \right) + \left(1 - e^{-\frac{b-y}{\lambda_0 \sin \theta \sin \Phi}} \right) \right\} d\Phi \\
& - \int_{\Phi=\tan^{-1}(\frac{b-y}{x})}^{\frac{\pi}{2}} \left\{ \left(1 - e^{-\frac{y}{\lambda_0 \sin \theta \sin \Phi}} \right) + \left(1 - e^{-\frac{y}{\lambda_0 \sin \theta \sin \Phi}} \right) + \left(1 - e^{-\frac{x}{\lambda_0 \sin \theta \cos \Phi}} \right) + \left(1 - e^{-\frac{b-y}{\lambda_0 \sin \theta \sin \Phi}} \right) \right\} d\Phi \\
& + \int_{\Phi=\tan^{-1}(\frac{b-y}{x})}^{\frac{\pi}{2}} \left\{ \left(1 - e^{-\frac{y}{\lambda_0 \sin \theta \sin \Phi}} \right) + \left(1 - e^{-\frac{y}{\lambda_0 \sin \theta \sin \Phi}} \right) + \left(1 - e^{-\frac{b-y}{\lambda_0 \sin \theta \sin \Phi}} \right) + \left(1 - e^{-\frac{b-y}{\lambda_0 \sin \theta \sin \Phi}} \right) \right\} d\Phi
\end{aligned} \tag{a2}$$

in one of the four sub-expressions. By summing the second and third expressions, we obtain

$$\int_{\tan^{-1}(\frac{y}{a-x})}^{\frac{\pi}{2}} \left(e^{-\frac{y}{\lambda_0 \sin \theta \sin \Phi}} - e^{-\frac{a-x}{\lambda_0 \sin \theta \cos \Phi}} \right) d\Phi \tag{a3}$$

Similarly, adding fourth and fifth expression, we get

$$\int_{\tan^{-1}(\frac{y}{x})}^{\frac{\pi}{2}} \left(e^{-\frac{y}{\lambda_0 \sin \theta \sin \Phi}} - e^{-\frac{x}{\lambda_0 \sin \theta \cos \Phi}} \right) d\Phi \tag{a4}$$

Repeating this for the sixth and seventh expression together yields

$$\int_{\tan^{-1}(\frac{b-y}{a-x})}^{\frac{\pi}{2}} \left(e^{-\frac{b-y}{\lambda_0 \sin \theta \sin \Phi}} - e^{-\frac{a-x}{\lambda_0 \sin \theta \cos \Phi}} \right) d\Phi \tag{a5}$$

Lastly, for the eighth and ninth expression, we get

$$\int_{\tan^{-1}(\frac{b-y}{x})}^{\frac{\pi}{2}} \left(e^{-\frac{b-y}{\lambda_0 \sin \theta \sin \Phi}} - e^{-\frac{x}{\lambda_0 \sin \theta \cos \Phi}} \right) d\Phi \tag{a6}$$

Also, the first expression in (a1) can be rewritten as

$$\begin{aligned}
& 4 \int_{\Phi=0}^{\frac{\pi}{2}} d\Phi - 4 \int_{\Phi=0}^{\frac{\pi}{2}} e^{-\frac{a}{2\lambda_0 \sin \theta \cos \Phi}} \\
& \quad \times \cosh \left(\frac{x - a/2}{\lambda_0 \sin \theta \cos \Phi} \right) d\Phi
\end{aligned} \tag{a7}$$

Combining (a3) - (a7), the η function can be simplified as follow

$$\begin{aligned}
\eta(x, y, \theta) &= 4 \int_{\Phi=0}^{\frac{\pi}{2}} d\Phi \\
& - 4 \int_{\Phi=0}^{\frac{\pi}{2}} e^{-\frac{a}{2\lambda_0 \sin \theta \cos \Phi}} \times \cosh \left(\frac{x - a/2}{\lambda_0 \sin \theta \cos \Phi} \right) d\Phi \\
& - \left\{ \int_{\tan^{-1}(\frac{y}{a-x})}^{\frac{\pi}{2}} \left(e^{-\frac{y}{\lambda_0 \sin \theta \sin \Phi}} - e^{-\frac{a-x}{\lambda_0 \sin \theta \cos \Phi}} \right) d\Phi \right. \\
& + \int_{\tan^{-1}(\frac{y}{x})}^{\frac{\pi}{2}} \left(e^{-\frac{y}{\lambda_0 \sin \theta \sin \Phi}} - e^{-\frac{x}{\lambda_0 \sin \theta \cos \Phi}} \right) d\Phi \\
& + \int_{\tan^{-1}(\frac{b-y}{a-x})}^{\frac{\pi}{2}} \left(e^{-\frac{b-y}{\lambda_0 \sin \theta \sin \Phi}} - e^{-\frac{a-x}{\lambda_0 \sin \theta \cos \Phi}} \right) d\Phi \\
& \left. + \int_{\tan^{-1}(\frac{b-y}{x})}^{\frac{\pi}{2}} \left(e^{-\frac{b-y}{\lambda_0 \sin \theta \sin \Phi}} - e^{-\frac{x}{\lambda_0 \sin \theta \cos \Phi}} \right) d\Phi \right\}
\end{aligned} \tag{a8}$$

If we look at the terms within the curly bracket, the order of the boundary points does not matter. The expression is only a

$$\begin{aligned}
\eta(x, y, \theta) &= \int_{\Phi=0}^{\tan^{-1}(\frac{y}{a-x})} \left\{ \left(1 - e^{-\frac{x}{\lambda_0 \sin \theta \cos \Phi}} \right) + \left(1 - e^{-\frac{a-x}{\lambda_0 \sin \theta \cos \Phi}} \right) + \left(1 - e^{-\frac{x}{\lambda_0 \sin \theta \cos \Phi}} \right) + \left(1 - e^{-\frac{a-x}{\lambda_0 \sin \theta \cos \Phi}} \right) \right\} d\Phi \\
& - \int_{\Phi=0}^{\tan^{-1}(\frac{y}{a-x})} \left\{ \left(1 - e^{-\frac{x}{\lambda_0 \sin \theta \cos \Phi}} \right) + \left(1 - e^{-\frac{y}{\lambda_0 \sin \theta \sin \Phi}} \right) + \left(1 - e^{-\frac{x}{\lambda_0 \sin \theta \cos \Phi}} \right) + \left(1 - e^{-\frac{a-x}{\lambda_0 \sin \theta \cos \Phi}} \right) \right\} d\Phi \\
& + \int_{\Phi=0}^{\tan^{-1}(\frac{y}{x})} \left\{ \left(1 - e^{-\frac{x}{\lambda_0 \sin \theta \cos \Phi}} \right) + \left(1 - e^{-\frac{y}{\lambda_0 \sin \theta \sin \Phi}} \right) + \left(1 - e^{-\frac{x}{\lambda_0 \sin \theta \cos \Phi}} \right) + \left(1 - e^{-\frac{a-x}{\lambda_0 \sin \theta \cos \Phi}} \right) \right\} d\Phi \\
& - \int_{\Phi=0}^{\tan^{-1}(\frac{y}{x})} \left\{ \left(1 - e^{-\frac{y}{\lambda_0 \sin \theta \sin \Phi}} \right) + \left(1 - e^{-\frac{y}{\lambda_0 \sin \theta \sin \Phi}} \right) + \left(1 - e^{-\frac{x}{\lambda_0 \sin \theta \cos \Phi}} \right) + \left(1 - e^{-\frac{a-x}{\lambda_0 \sin \theta \cos \Phi}} \right) \right\} d\Phi \\
& + \int_{\Phi=0}^{\tan^{-1}(\frac{b-y}{a-x})} \left\{ \left(1 - e^{-\frac{y}{\lambda_0 \sin \theta \sin \Phi}} \right) + \left(1 - e^{-\frac{y}{\lambda_0 \sin \theta \sin \Phi}} \right) + \left(1 - e^{-\frac{x}{\lambda_0 \sin \theta \cos \Phi}} \right) + \left(1 - e^{-\frac{a-x}{\lambda_0 \sin \theta \cos \Phi}} \right) \right\} d\Phi \\
& - \int_{\Phi=0}^{\tan^{-1}(\frac{b-y}{a-x})} \left\{ \left(1 - e^{-\frac{y}{\lambda_0 \sin \theta \sin \Phi}} \right) + \left(1 - e^{-\frac{y}{\lambda_0 \sin \theta \sin \Phi}} \right) + \left(1 - e^{-\frac{x}{\lambda_0 \sin \theta \cos \Phi}} \right) + \left(1 - e^{-\frac{b-y}{\lambda_0 \sin \theta \sin \Phi}} \right) \right\} d\Phi
\end{aligned} \tag{a9}$$

> REPLACE THIS LINE WITH YOUR MANUSCRIPT ID NUMBER (DOUBLE-CLICK HERE TO EDIT) <

$$\begin{aligned} \eta &+ \int_{\Phi=0}^{\tan^{-1}(\frac{b-y}{x})} \left\{ \left(1 - e^{-\frac{y}{\lambda_0 \sin \theta \sin \Phi}}\right) + \left(1 - e^{-\frac{y}{\lambda_0 \sin \theta \sin \Phi}}\right) + \left(1 - e^{-\frac{x}{\lambda_0 \sin \theta \cos \Phi}}\right) + \left(1 - e^{-\frac{b-y}{\lambda_0 \sin \theta \sin \Phi}}\right) \right\} d\Phi \\ &- \int_{\Phi=0}^{\tan^{-1}(\frac{b-y}{x})} \left\{ \left(1 - e^{-\frac{y}{\lambda_0 \sin \theta \sin \Phi}}\right) + \left(1 - e^{-\frac{y}{\lambda_0 \sin \theta \sin \Phi}}\right) + \left(1 - e^{-\frac{b-y}{\lambda_0 \sin \theta \sin \Phi}}\right) + \left(1 - e^{-\frac{b-y}{\lambda_0 \sin \theta \sin \Phi}}\right) \right\} d\Phi \\ &+ \int_{\Phi=0}^{\frac{\pi}{2}} \left\{ \left(1 - e^{-\frac{y}{\lambda_0 \sin \theta \sin \Phi}}\right) + \left(1 - e^{-\frac{y}{\lambda_0 \sin \theta \sin \Phi}}\right) + \left(1 - e^{-\frac{b-y}{\lambda_0 \sin \theta \sin \Phi}}\right) + \left(1 - e^{-\frac{b-y}{\lambda_0 \sin \theta \sin \Phi}}\right) \right\} d\Phi \end{aligned} \quad (a9)$$

$$\begin{aligned} \eta(x, y, \theta) &= 4 \int_{\Phi=0}^{\frac{\pi}{2}} d\Phi - 4 \int_{\Phi=0}^{\frac{\pi}{2}} e^{-\frac{b}{2\lambda_0 \sin \theta \sin \Phi}} \times \cosh\left(\frac{y-b/2}{\lambda_0 \sin \theta \sin \Phi}\right) d\Phi \\ &- \left\{ \int_{\tan^{-1}(0)}^{\tan^{-1}(\frac{b-y}{x})} \left(e^{-\frac{x}{\lambda_0 \sin \theta \cos \Phi}} - e^{-\frac{b-y}{\lambda_0 \sin \theta \sin \Phi}} \right) d\Phi + \int_{\tan^{-1}(0)}^{\tan^{-1}(\frac{b-y}{a-x})} \left(e^{-\frac{a-x}{\lambda_0 \sin \theta \cos \Phi}} - e^{-\frac{b-y}{\lambda_0 \sin \theta \sin \Phi}} \right) d\Phi \right. \\ &\left. + \int_{\tan^{-1}(0)}^{\tan^{-1}(\frac{y}{x})} \left(e^{-\frac{x}{\lambda_0 \sin \theta \cos \Phi}} - e^{-\frac{y}{\lambda_0 \sin \theta \sin \Phi}} \right) d\Phi + \int_{\tan^{-1}(0)}^{\tan^{-1}(\frac{y}{a-x})} \left(e^{-\frac{a-x}{\lambda_0 \sin \theta \cos \Phi}} - e^{-\frac{y}{\lambda_0 \sin \theta \sin \Phi}} \right) d\Phi \right\} \end{aligned} \quad (a10)$$

function of the boundary points. Thus, this η expression holds true for the other seven regions as well.

Recall, when we transformed (a1) to (a2), we make the upper limits of all the integrals to be $\frac{\pi}{2}$ and then combine the expressions. We can also follow a similar process but make the lower limit of the integrals to be 0. When we do that, (a1) translates to (a9) in the similar manner as shown (a9).

By adding first and second, third and fourth, fifth and sixth, and seventh and eighth expressions in pairs together, and rewriting the ninth expression in terms of cosh (similar to (a7)), we can get another expression for η function as below (a10).

For symmetry, we add (a8) and (a10) together and divide by 2 to get the final expression (a11 next page).

Here the n and d define the four boundary points. Note, when we combine (a8) and (a10), we add the two integrals corresponding to the same boundary point in the upper/lower limit of integration to obtain the final integral with $\Phi = 0 \rightarrow \pi/2$. It is noteworthy that the corresponding integrand is the same except for a negative sign. Also, the integrand is always positive, as dictated by the *min* function in (15). Hence, we use the absolute value of $(e^{-\frac{d}{\lambda_0 \sin \theta \cos \Phi}} - e^{-\frac{n}{\lambda_0 \sin \theta \sin \Phi}})$ and combine the integrals to obtain the final expression in (a11). This approach is also valid for a general p .

$$\begin{aligned} \eta(x, y, \theta) &= 2\pi \\ &- 2 \int_{\Phi=0}^{\frac{\pi}{2}} \left\{ e^{-\frac{b}{2\lambda_0 \sin \theta \sin \Phi}} \times \cosh\left(\frac{y-\frac{b}{2}}{\lambda_0 \sin \theta \sin \Phi}\right) \right. \\ &\left. + e^{-\frac{a}{2\lambda_0 \sin \theta \cos \Phi}} \times \cosh\left(\frac{x-\frac{a}{2}}{\lambda_0 \sin \theta \cos \Phi}\right) d\Phi \right\} \quad (a11) \\ &- \frac{1}{2} \sum_{n,d} \int_{\Phi=0}^{\frac{\pi}{2}} \left| e^{-\frac{d}{\lambda_0 \sin \theta \cos \Phi}} - e^{-\frac{n}{\lambda_0 \sin \theta \sin \Phi}} \right| d\Phi \end{aligned}$$

where $(n, d) \rightarrow \{(y, x), (y, a-x), (b-y, x), (b-y, a-x)\}$

APPENDIX A2

For validating the SRFS model, we use the models¹³ for a square wire (of height=width= a). The authors²¹ have derived various simplified expressions for various κ ($\kappa = a/\lambda_0$), which we utilize for comparison in Fig. 4. We list these approximations from (4) for the convenience of the readers.

$$\frac{\sigma}{\sigma_0} = \frac{3}{4} \kappa \log_e \left(\frac{\sqrt{2}+1}{\sqrt{2}-1} \right) - \frac{1}{2} \kappa (\sqrt{2} - 1) \quad \text{for } \kappa < 0.2 \quad (a12)$$

$$\begin{aligned} \frac{\sigma}{\sigma_0} &= 1 - \frac{3}{\pi} \left(\frac{\pi}{4\kappa} - \frac{4}{15\kappa^2} \right) \\ &+ \frac{12}{\pi} \int_0^{\frac{\pi}{2}} \left(\frac{\pi \cos \theta}{4\kappa} \right. \\ &\left. - \frac{\kappa \sin \theta - \sin 2\theta}{3\kappa^2} \right) e^{-\frac{\kappa}{\cos \theta}} \sin^3 \theta d\theta \\ &+ \frac{12}{\pi} \int_{\frac{\pi}{4}}^{\frac{\pi}{2}} \left(\frac{\cos \theta}{\kappa} \left(\frac{\pi}{4} - \frac{\cos(\cot \theta)^{-1}}{2} \right) + \right. \end{aligned} \quad (a13)$$

$$\begin{aligned} &\left. \frac{\cot^2 \theta}{2\kappa} \sqrt{(-\cos 2\theta)} - \frac{\sin \theta - (-\cos 2\theta)^{3/2} / \sin^2 \theta}{3\kappa} \right) \\ &\left. \frac{2}{3\kappa^2} (\sin \theta \cos \theta - \frac{\cos \theta}{\sin^2 \theta} (-\cos 2\theta)^{3/2}) \right) e^{-\frac{\kappa}{\cos \theta}} \sin^3 \theta d\theta \\ &\text{for } 0.2 < \kappa < 4 \end{aligned}$$

$$\begin{aligned} \frac{\sigma}{\sigma_0} &= 1 - \frac{6}{\pi} \left(\frac{\pi}{8\kappa} - \frac{2}{15\kappa^2} \right) + \\ &\frac{12}{\pi\kappa} \int_{\theta=0}^{\frac{\pi}{2}} \int_{\phi=0}^{\frac{\pi}{4}} e^{-\frac{\kappa}{\sin \theta \cos \phi}} \cos \phi \sin^2 \theta \cos^2 \theta d\theta d\phi + \\ &\frac{12}{\pi\kappa^2} \int_{\theta=0}^{\frac{\pi}{2}} \left(\frac{e^{-\sqrt{2}\kappa/\sin \theta}}{2} - e^{-\kappa/\sin \theta} \right) \sin^3 \theta \cos^2 \theta d\theta \\ &\text{for } \kappa > 4 \end{aligned} \quad (a14)$$

Note, (a14) can be further simplified to $\frac{\sigma}{\sigma_0} \approx 1 - \frac{0.75}{\kappa} + \frac{0.254}{\kappa^2}$. A variation of this simplified expression has been used in many pervious works^{16,25,29,30}. However, this simplified expression must be used only for cases that $\kappa > 4$, as also pointed out in here¹⁹.

ACKNOWLEDGMENT

This work was supported, in part, by SRC/NIST-funded NEWLIMITS Center (Award number 70NANB17H041)

REFERENCES

- ¹ B. Yu, L. Chang, S. Ahmed, H. Wang, S. Bell, C.-Y. Yang, C. Tabery, C. Ho, Q. Xiang, T.-J. King, J. Bokor, C. Hu, M.-R. Lin, and D. Kyser, in *Digest. International Electron Devices Meeting*, (2002), pp. 251–254.
- ² J. Ajayan, D. Nirmal, S. Tayal, S. Bhattacharya, L. Arivazhagan, A.S.A. Fletcher, P. Murugapandiyam, and D. Ajitha, “Nanosheet field effect transistors-A next generation device to keep Moore’s law alive: An intensive study,” *Microelectronics J* **114**, 105141 (2021).
- ³ R. Brain, in *2016 IEEE International Electron Devices Meeting (IEDM)* (2016), pp. 9.3.1–9.3.4.
- ⁴ R.L. Graham, G.B. Alers, T. Mountsier, N. Shamma, S. Dhuey, S. Cabrini, R.H. Geiss, D.T. Read, and S. Peddetti, “Resistivity dominated by surface scattering in sub-50 nm Cu wires,” *Appl Phys Lett* **96**(4), (2010).
- ⁵ W.L. Wang, C.T. Wang, W.C. Chen, K.T. Peng, M.H. Yeh, H.C. Kuo, H.J. Chien, J.C. Chuang, and T.H. Ying, “The Reliability Improvement of Cu Interconnection by the Control of Crystallized α -Ta/TaN_x Diffusion Barrier,” *J Nanomater* **2015**, (2015).
- ⁶ D. Edelstein, C. Uzoh, C. Cabral, P. DeHaven, P. Buchwalter, A. Simon, E. Cooney, S. Malhotra, D. Klaus, H. Rathore, B. Agarwala, and D. Nguyen, in *Proceedings of the IEEE 2001 International Interconnect Technology Conference (Cat. No.01EX461)* (2001), pp. 9–11.
- ⁷ N. Bekiaris, Z. Wu, H. Ren, M. Naik, J.H. Park, M. Lee, T.H. Ha, W. Hou, J.R. Bakke, M. Gage, Y. Wang, and J. Tang, in *2017 IEEE International Interconnect Technology Conference (IITC)* (2017), pp. 1–3.
- ⁸ D. Wan, S. Paolillo, N. Rassoul, B.K. Kotowska, V. Blanco, C. Adelman, F. Lazzarino, M. Ercken, G. Murdoch, J. Bömmels, C.J. Wilson, and Z. Tökei, in *2018 IEEE International Interconnect Technology Conference (IITC)* (2018), pp. 10–12.
- ⁹ T.M. Philip, N.A. Lanzillo, T. Gunst, T. Markussen, J. Cobb, S. Aboud, and R.R. Robison, “First-Principles Evaluation of fcc Ruthenium for its use in Advanced Interconnects,” *Phys Rev Appl* **13**(4), (2020).
- ¹⁰ C.L. Lo, B.A. Helfrecht, Y. He, D.M. Guzman, N. Onofrio, S. Zhang, D. Weinstein, A. Strachan, and Z. Chen, “Opportunities and challenges of 2D materials in back-end-of-line interconnect scaling,” *J Appl Phys* **128**(8), (2020).
- ¹¹ B. Grot, J. Hestness, S.W. Keckler, and O. Mutlu, in *2009 IEEE 15th International Symposium on High Performance Computer Architecture* (2009), pp. 163–174.
- ¹² E.H. SONDHEIMER, “Influence of a Magnetic Field on the Conductivity of Thin Metallic Films,” *Nature* **164**(4178), 920–921 (1949).
- ¹³ D.K.C. Macdonald, and K. Sarginson, *Size Effect Variation of the Electrical Conductivity of Metals* (1950).
- ¹⁴ R.B. Dingle, and W.L. Bragg, “The electrical conductivity of thin wires,” *Proc R Soc Lond A Math Phys Sci* **201**(1067), 545–560 (1950).
- ¹⁵ A.F. Mayadas, and M. Shatzkes, “Electrical-Resistivity Model for Polycrystalline Films: the Case of Arbitrary Reflection at External Surfaces,” *Phys Rev B* **1**(4), 1382–1389 (1970).
- ¹⁶ R. Mehta, S. Chugh, and Z. Chen, “Enhanced electrical and thermal conduction in graphene-encapsulated copper nanowires,” *Nano Lett* **15**(3), 2024–2030 (2015).
- ¹⁷ T. Shen, D. Valencia, Q. Wang, K.C. Wang, M. Povolotskiy, M.J. Kim, G. Klimeck, Z. Chen, and J. Appenzeller, “MoS₂ for Enhanced Electrical Performance of Ultrathin Copper Films,” *ACS Appl Mater Interfaces* **11**(31), 28345–28351 (2019).
- ¹⁸ X. Chen, C.-L. Lo, M.C. Johnson, Z. Chen, and S.K. Gupta, in *2021 Device Research Conference (DRC)* (2021), pp. 1–2.
- ¹⁹ R.G. Chambers, *The Conductivity of Thin Wires in a Magnetic Field* (1950).
- ²⁰ L. Moraga, C. Arenas, R. Henriquez, and B. Solis, “The effect of surface roughness and grain-boundary scattering on the electrical conductivity of thin metallic wires,” *Phys Status Solidi B Basic Res* **252**(1), 219–229 (2015).
- ²¹ E.H. Sondheimer, “The mean free path of electrons in metals,” *Adv Phys* **1**(1), 1–42 (1952).
- ²² T. Lu, and A. Srivastava, in *2013 IEEE International 3D Systems Integration Conference (3DIC)* (2013), pp. 1–7.
- ²³ I. Ciofi, A. Contino, P.J. Roussel, R. Baert, V.H. Vega-Gonzalez, K. Croes, M. Badaroglu, C.J. Wilson, P. Raghavan, A. Mercha, D. Verkest, G. Groeseneken, D. Mocuta, and A. Thean, “Impact of Wire Geometry on Interconnect RC and Circuit Delay,” *IEEE Trans Electron Devices* **63**(6), 2488–2496 (2016).
- ²⁴ W. Steinhögl, G. Schindler, G. Steinlesberger, and M. Engelhardt, “Size-dependent resistivity of metallic wires in the mesoscopic range,” *Phys Rev B Condens Matter Phys* **66**(7), 1–4 (2002).
- ²⁵ R. Saligram, S. Datta, and A. Raychowdhury, “Scaled Back End of Line Interconnects at Cryogenic Temperatures,” *IEEE Electron Device Letters* **42**(11), 1674–1677 (2021).
- ²⁶ J.S. Chawla, F. Gstrein, K.P. O’Brien, J.S. Clarke, and D. Gall, “Electron scattering at surfaces and grain boundaries in Cu thin films and wires,” *Phys Rev B Condens Matter Mater Phys* **84**(23), (2011).
- ²⁷ R.S. Smith, E.T. Ryan, C.K. Hu, K. Motoyama, N. Lanzillo, D. Metzler, L. Jiang, J. Demarest, R. Quon, L. Gignac, C. Breslin, A. Giannetta, and S. Wright, “An evaluation of Fuchs-Sondheimer and Mayadas-Shatzkes models below 14nm node wide lines,” *AIP Adv* **9**(2), (2019).
- ²⁸ D. Gall, “The search for the most conductive metal for narrow interconnect lines,” *J Appl Phys* **127**(5), (2020).
- ²⁹ N.C. Wang, S. Sinha, B. Cline, C.D. English, G. Yeric, and E. Pop, in *2017 IEEE International Interconnect Technology Conference (IITC)* (2017), pp. 1–3.
- ³⁰ A. Pyzyna, R. Bruce, M. Lofaro, H. Tsai, C. Witt, L. Gignac, M. Brink, M. Guillorn, G. Fritz, H. Miyazoe, D. Klaus, E. Joseph, K.P. Rodbell, C. Lavoie, and D.-G. Park, *Resistivity of Copper Interconnects beyond the 7 Nm Node* (2015).